Corrosion inhibition of steel in seawater through surface phosphate formed from oil

Jeffrey Poon[1], David C. Madden[1], Rebecca J. L. Welbourn[2], Finian J. Allen[1], Fahmida Khan[1], Hans Sonke[3], Stuart M. Clarke*[1]

[1] BP Institute and Department of Chemistry, University of Cambridge, Cambridge, CB3 0EZ, UK

[2] ISIS Neutron and Muon Source, Science and Technology Facilities Council, Rutherford Appleton Laboratory, Didcot, OX11 0QX, UK

[3] Shell Global Research Centre, Amsterdam, The Netherlands

*Corresponding author: stuart@bpi.cam.ac.uk; +44 (0) 1223 765700

Keywords: phosphate; steel; corrosion; water exposure; surface analysis, neutron reflectometry

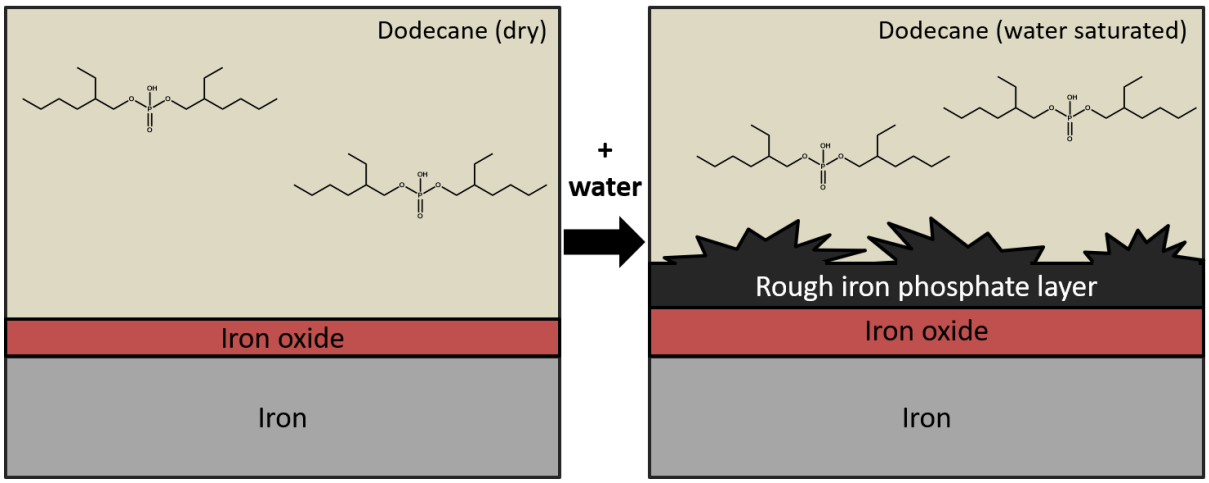

Abstract

Bis(2-ethylhexyl) phosphate (BEHP) was exposed to carbon steel surfaces from dry and water-saturated dodecane. The resulting changes to the surfaces were characterised using spectroscopic techniques (energy dispersive X-ray (EDX), X-ray photoelectron (XPS), and far-infrared reflection absorption (RAIRS) spectroscopies) and polarised neutron reflectometry (PNR). Although there was no observable affinity of BEHP to the steel surface in dry solvent, a layer of rough iron (III) phosphate formed in water-saturated dodecane. The phosphate-reacted steel surface showed some resistance to corrosion by seawater, suggesting the formation of a cohesive barrier against corrosive species. The results support the use of BEHP as an anti-corrosion additive and a viable phosphating agent for steel surfaces.

1. Introduction

The adsorption of additives to solid surfaces from liquids is key to many commercial and industrial processes, from engine lubrication using fatty acids to enhanced oil recovery.[1–3] Many investigations relating to adsorption concern corrosion, which can contaminate and significantly undermine the designed properties of materials,[4] and which therefore has a high economic and safety impact.[5,6] Although there are many papers studying adsorption on metals or their associated oxides,[7–16] corrosion prevention on different metal substrates remains a complicated problem, due to the large variety of corrosive environments. Efforts have recently been made to monitor corrosion and adsorption at early stages of the process, so relevant surfaces can be targeted for corrective treatment and/or protected prior to repainting.[17–19] Similarly, the initiation of the corrosion

process has been observed through *in situ* observations, including electron microscopy,[20,21] optical spectroscopy,[22] electrochemistry,[23] and synchrotron techniques and neutron reflectometry.[24–26] Understanding the mechanisms of corrosion initiation allows corrosion to be arrested as soon as possible.

Carbon steel is a commonly used structural material for architectural and engineering purposes. Corrosion of steel has been addressed through different surface treatments, such as galvanisation with zinc,[27] or using chromate salts,[5] surface silanation,[28] or surface phosphating.[29] Application of organic coatings (i.e. paint), in which many organic additives and binder materials are mixed,[30,31] remains one of the most popular methods to attempt to stop or delay corrosion. In recent years, there has been increasing focus in developing more environmentally friendly and sustainable corrosion inhibitors, as well as theoretical rationalisations and predictions of inhibitor effects.[32] These inhibitors can be derived from many organic (surfactants, biopolymers, amino acids, etc.) and inorganic (metal ions) sources. Amino acid-derived corrosion inhibitors have received significant attention due to their environmental compatibility.[33] Synergetic approaches of using a combination of corrosion inhibitors have also been explored in broad scope, with zinc-ion-containing formulations behaving as a mixed corrosion inhibitor, inhibiting both anodic and cathodic corrosion reactions.[34] All of the above methods are reported to work by forming a passivating layer on the steel, to prevent or retard corrosive species reaching the steel, or by stopping the reaction at either/both corrosion half-cell.

The phosphating of steel surfaces for corrosion resistance is based on the formation of a cohesive, insoluble phosphate layer to improve corrosion and wear resistance. The evolution of surface phosphating technology includes the use of organic phosphate compounds, most notably zinc dialkyldithiophosphates (ZDDPs), which are activated tribologically, forming a phosphate glass that improves wear resistance of mechanical parts.[35–37] Bis(2-ethylhexyl) phosphate (BEHP) has been shown to form self-assembled films that have the potential to inhibit corrosion under aqueous conditions.[38] BEHP also has particular affinity for ferric ions and can be used to transfer ions from an aqueous phase to an organic phase.[39] As such, it is important to better understand the nature of the reaction BEHP has with carbon steel. If BEHP can be applied via a surface treatment and act as a phosphating agent without requiring total immersion of the steel parts, this would make it an attractive anti-corrosion solution for large carbon steel components, such as those used in shipbuilding or on offshore structures. This work investigates the interaction between BEHP and steel at the aliphatic solvent-steel interface, relevant to painting conditions.

2. Experimental

2.1. Chemicals and reagents

Bis(2-ethylhexyl) phosphate (BEHP, 97%) and n-hexane (referred to as 'hexane' henceforth, ≥ 99%) were supplied by Sigma Aldrich and were used without further purification. The molecular structure of BEHP is shown in Figure 1. n-Dodecane (referred to as 'dodecane' henceforth, ≥ 99%) was supplied by Merck, while d_{26}-dodecane (d-dodecane, ≥ 98% deuteration) from Sigma Aldrich was supplied by the Deuteration Facility at the ISIS Neutron and Muon Source, Didcot, UK. The d-dodecane was dried with molecular sieves prior to use. Heavy water (D_2O, 99.9% deuteration) was also supplied by Sigma Aldrich. The 'dried' dodecane had 15.0 ± 2.2 ppm water content, as determined through Karl Fischer titration,[40] and a water-saturated 'wet' dodecane had 55.1 ± 3.0 ppm water content, close to the literature quoted limit of 65 ppm at room temperature.[41] This range of dissolved water is the widest range of water content that it is practical to employ in the absence of more rigorous systems (e.g. dosing water under UHV conditions). In this work, even over this narrow range there are observable differences in BEHP-iron interactions, which will be explored in detail in Results and Discussion.

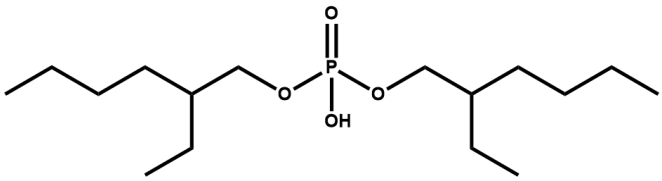

Figure 1: Molecular structure of bis(2-ethylhexyl) phosphate (BEHP)

S355 carbon steel coupons and powder were supplied by Parker Steel, Canterbury, UK and Sandvik Osprey, Neath, UK, respectively. The bulk elemental composition of S355 coupons from the manufacturer are quoted in Table SI1 in the Supporting Information. The polished steel coupons and powdered substrate have been characterised previously;[42] BET analysis indicated a specific surface area for the powder of 0.30 ± 0.06 m^2g^{-1}. Coupons were polished using successive grades of Kemet (Maidstone, Kent) diamond compound (25, 10, 5, and 1 µm) until a mirror finish was achieved. The substrate was then sonicated in 2% Neutracon (Decon Laboratories, Hove, UK) solution for 1 min, rinsed 10 times with 50 mL ultrapure water, sonicated in ultrapure water for 1 min, then finally rinsed 10 times more with ultrapure water. The surface was blown dry with a jet of dry nitrogen.

2.2. Scanning electron microscope-energy dispersive spectroscopy (SEM-EDX)

Micrographs were collected using a JEOL Model JSM 6360LV instrument with an Oxford Instruments Inca EDS attachment, at the Department of Chemistry, University of Cambridge, UK. Higher resolution images were collected using a FEI QEMSCAN 650F with a Bruker QUANTEX EDS attachment at the Department of Earth Sciences, University of Cambridge.

2.3. X-ray photoelectron spectroscopy (XPS)

Spectra were collected using a Thermo Fisher ESCALAB 250Xi instrument, with monochromatic aluminium source (1486.68 eV), at the Cavendish Laboratory, University of Cambridge. The analysis area was defined by the incident X-ray beam, which was micro-focused to a 400 µm diameter spot on the sample surface, with the detector positioned to collect electrons emitted at 90° to the surface. Two spots are sampled across each sample surface. Detailed survey spectra were collected at a pass energy of 50 eV. Detailed spectral analysis was conducted using CasaXPS software, with the alkyl carbon peak (C−C) at 284.8 eV binding energy as a reference, to deconvolute the components contributing to peaks. All fittings use 70% Gaussian and 30% Lorentzian peaks (GL(30) setting), except for metallic species, for which asymmetrical Gaussian-Lorentzian peaks were used. Backgrounds were generated with the Shirley method if the intensity of the spectrum was higher at higher binding energies; if not, linear backgrounds were used.[43,44]

2.4. Far-infrared reflection absorption infrared spectroscopy (far-IR RAIRS)

Spectra were collected at the B22 instrument, Diamond Light Source, Didcot, UK, using a Bruker Vertex 80V spectrometer with a glowing source. A shallow incidence (80° to the surface normal) was used, as was a sampling aperture of 20 mm, to increase the footprint of the incoming beam. A Pike Technologies VeeMax II variable-angle specular reflection accessory controlled the angle of incidence. Once the sample was placed in the spectrometer, the sample chamber was pumped for 30 minutes, to give a chamber pressure no higher than 2 mbar. More than 126 scans per sample were made for each scanning session, to obtain a signal-to-noise ratio no lower than 10,000 for the collected raw spectra. The detector was a helium-cooled bolometer. Sample spectra are all referenced to a background spectrum of a smooth gold mirror. Thermal vapour deposited iron films were used as a

model substrate for steel; these were immersed in 10 mM BEHP in dodecane (as purchased, no additional drying) for 24 hrs prior to measurements.

2.5. Polarised neutron reflectometry (PNR)

Reflectometry spectra were collected at the POLREF instrument at the ISIS Neutron and Muon Source. Details of the cell have been published previously,[16] as have details of the instrument.[45] The incident neutrons were reflected from the surface of interest using a polarised beam. Due to the relative reflected intensity observed for the two spin states in this sample, the count times were optimised as a 1:3 ratio for the lowest angle and 1:4 ratio for the higher angles. Magnetic yokes were used to impose an aligned magnetic field in the samples either parallel or antiparallel to the incoming polarised beam during data collection, yielding the up and down datasets. Spectra were collected at three different angles, 0.25°, 1.00°, and 2.3°, to give a momentum transfer, Q_z, range up to 0.20 $Å^{-1}$. The wavelength band of POLREF is 2 to 15 Å when polarised. Data were fitted using GenX software, written by Matts Björck and Gabriella Andersson,[46] with up- and down-spin co-fitting.[47,48]

N-type, silicon (111) wafer supports were polished by Crystran, Poole, UK to sub-nanometre roughness. The silicon wafers were then cleaned in concentrated (65%) nitric acid from Fisher Scientific for 24 hrs, rinsed with ample ultrapure water, soaked in ultrapure water for 24 hrs, rinsed again, and blown dry with a jet of dry nitrogen. Approximately 20 nm films of magnetron-sputtered iron were then deposited by the Material Growth Services at the Thin Film Magnetism Group, Cavendish Laboratory. The iron-deposited silicon wafers were stored in vacuum desiccators to prevent corrosion from atmospheric moisture and were only unsealed immediately prior to use. The neutron reflectivity was used to characterise the deposited films, as detailed in previous work and below.[26]

2.5. Electrochemical measurements

All electrochemical experiments were controlled using a Multi Autolab M204 in a three-electrode configuration. The 4 mm diameter circular S355 steel working electrode (WE) was encased in a polyether ether ketone (PEEK) sample holder. A platinum mesh (99.95%), supplied by Advent Research Materials Ltd, and a Gaskatel Mini HydroFlex reversible hydrogen electrode (RHE) were respectively used as the counter (CE) and reference electrode (RE). Corrosion experiments were conducted in 3.5 wt% artificial seawater made from sea salts supplied by Millipore. The pH of the solution, measured using Whatman pH strips, was 8.0 (± 0.5).[49]

The steel surface was renewed by sanding, first with P1000 then finished with P2000 silicon carbide sandpaper. Abrasive residue was removed from the electrode by 10 s sonication in hexane. The surface was then blown dry with a jet of compressed air. The S355 steel surface was modified by immersion in 2 mM BEHP in water-saturated dodecane for varying duration. The surface was then washed with 20 mL of hexane and blown dry.

The WE was exposed to stirred artificial seawater electrolyte, open to the atmosphere, for 30 min prior to electrochemical measurements, in order to obtain a steady-state corrosion potential (changing by less than 0.2 mV s^{-1}).[50] Linear polarisation curves were then conducted in the range ± 0.3 V of the corrosion potential, at a scan rate of 0.2 mV s^{-1} to minimise capacitive contributions to the current measured.

3. Results and Discussion

3.1. Visual observations

A polished S355 coupon, initially with a reflective mirror finish, was exposed to 10 mM BEHP in dodecane (as received) for 24 hrs, then washed with copious amounts of volatile hexane to remove

any excess dodecane solution. As shown in Figure 2, the coupon surface has significantly roughened, indicating a surface reaction. The reaction and altered surface texture were therefore investigated using a range of surface-sensitive techniques, as described below.

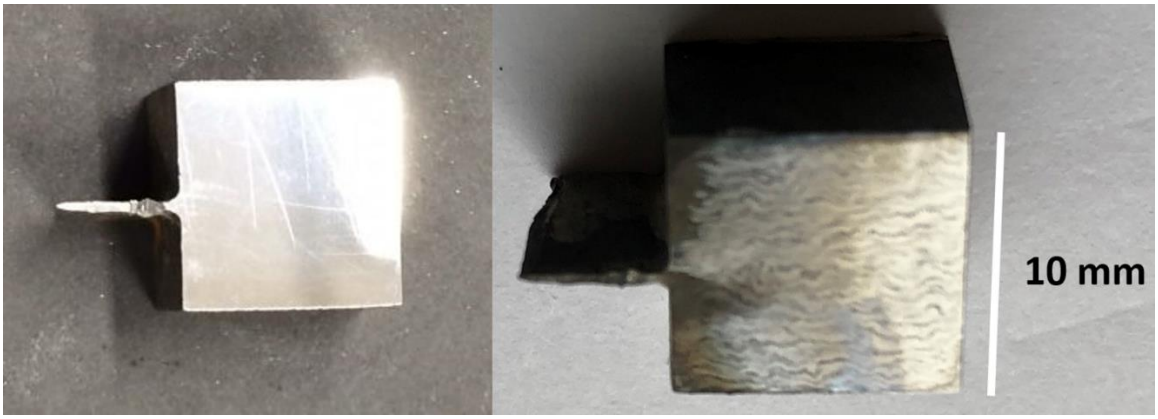

Figure 2: An S355 steel coupon before (left) and after (right) 24 hrs of exposure to 10 mM BEHP in 'wet' dodecane; the post-exposure surface is significantly roughened.

3.2. Scanning electron microscope-energy dispersive spectroscopy (SEM-EDX)

SEM analysis confirms significant topographic changes from the smooth, polished steel surface shown in Figure 3a, to the reacted surface after 24 hrs exposure to 10 mM BEHP in dodecane shown in Figure 3b. A large increase in roughness is confirmed from the contrast seen in the topographically-sensitive secondary electron micrograph. The EDX spectra comparison in Figure 4 (Figure 4c in particular) indicates an additional phosphorous peak on the post-exposure steel surface, confirming the inclusion of phosphorous. The EDX results are summarised Table 1. In addition to the appearance of the phosphorus peak, a significant rise in carbon and a decrease in iron atomic percentages are observed after exposure to the BEHP solution. These observations could suggest loss of iron, but more likely the obscuring of the steel by a deposited layer. Peaks are also evident corresponding to manganese, an alloying element in S355, and silicon; variable levels of silicon contamination are commonly observed on polished surfaces, due to the persistent surfactant in the diamond paste and lapping sprays used for lubrication.

Oxygen is not readily identified for the polished sample, although the very thin native iron oxide film has been characterised in previous work.[42] The oxygen Kα peak significantly overlaps with the large iron Lα peak, meaning that the low oxygen atomic percentage on the polished sample cannot be resolved. However, an oxygen peak is clearly evident as a shoulder on the iron peak after BEHP exposure, indicative of an increase in the surface oxygen content. The presence of the oxygen and phosphorus peaks in the post-exposure spectrum suggests that the reaction between S355 steel surface and BEHP (in dodecane) not only causes topographical changes, but also results a phosphate-containing product on the surface.

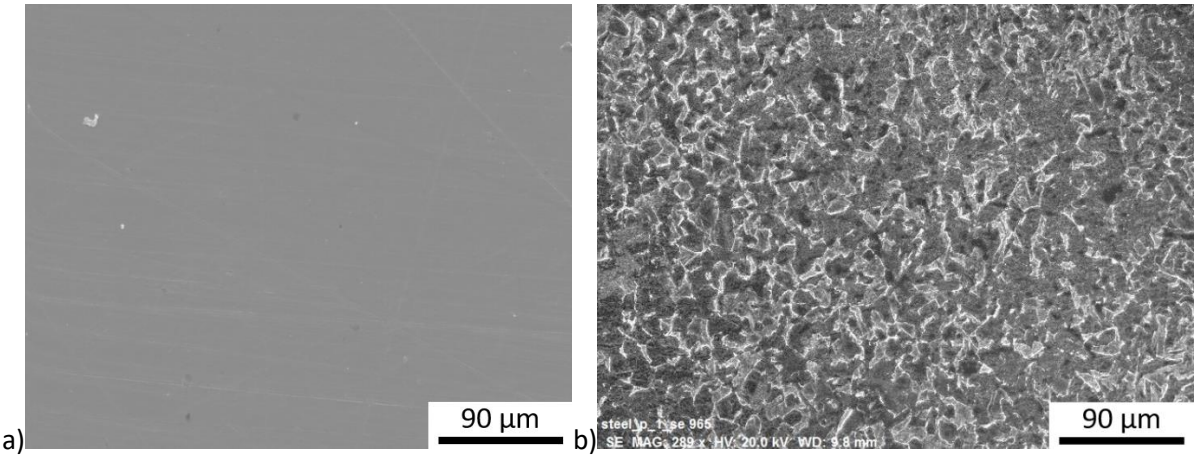

Figure 3: S355 steel surface under SEM inspection for a sample **a)** before and **b)** after exposure to 10 mM BEHP in 'wet' dodecane for 24 hrs

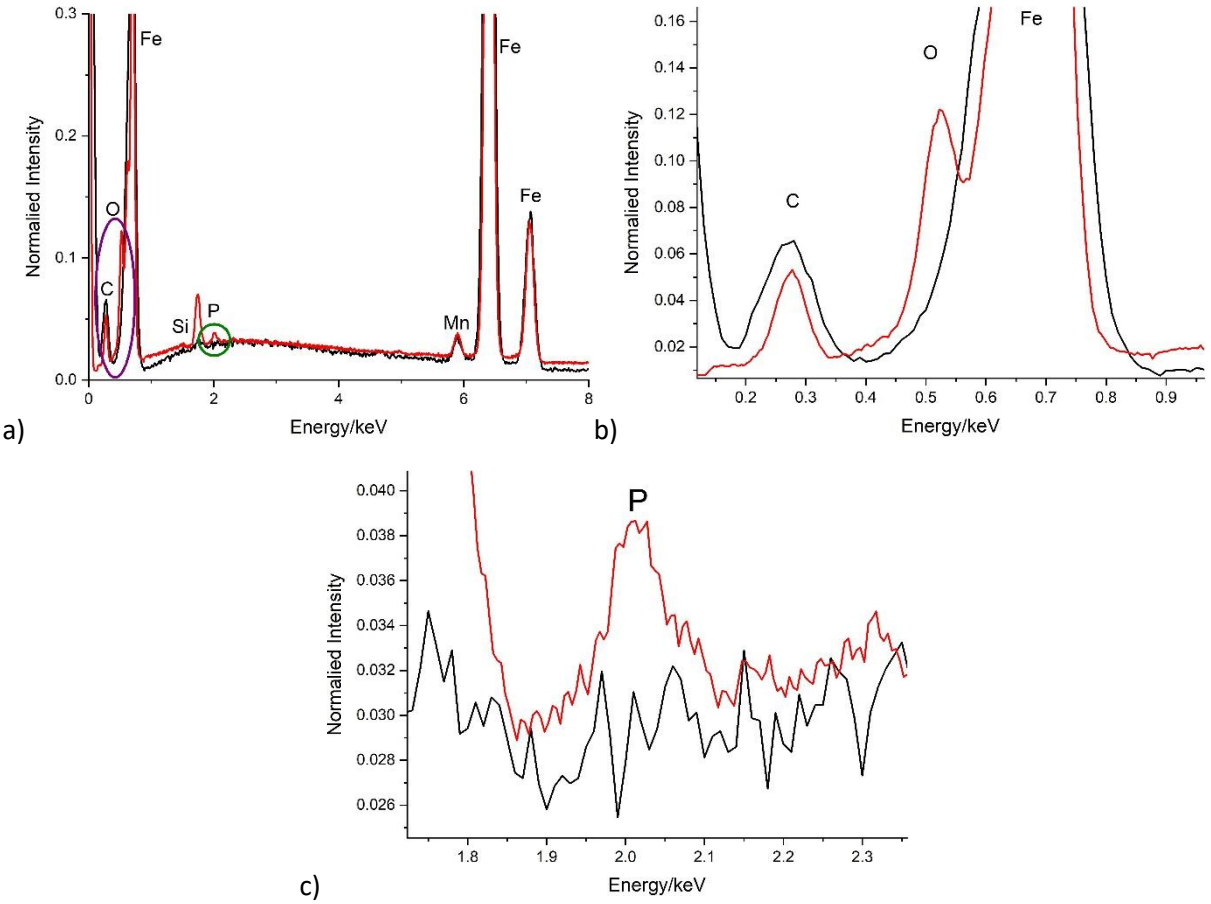

Figure 4: a) Direct comparison between EDX spectra obtained from polished S355 steel (black) and after the steel is exposed to 10 mM BEHP in 'wet' dodecane (red). The oxygen and phosphorous peaks are respectively circled in purple and green, with the corresponding regions expanded in **b)** and **c)**.

Element	EDX atomic percentage / %	
	Polished S355 steel	S355 after 10 mM BEHP exposure
C	13.9 ± 0.8	21.6 ± 2.8
O	0.0 ± 0.0	9.6 ± 4.4
Si	0.4 ± 0.0	1.3 ± 0.4

P	0.0 ± 0.0	0.2 ± 0.1
Mn	1.4 ± 0.1	1.1 ± 0.1
Fe	84.8 ± 2.6	66.1 ± 7.5

Table 1: Summary of EDX elemental analysis results for polished and 24-hour BEHP-exposed S355 steel. Errors are evaluated through collection of spectra from multiple sites.

3.3. X-ray photoelectron spectroscopy (XPS)

Further samples were analysed with XPS, to investigate the chemical environment of the phosphorous-containing product on the steel surface. Detailed scans were obtained for the iron 2p, carbon 1s, oxygen 1s, and phosphorous 2p regions, and analogous control scans were taken for steel samples immersed in pure dodecane for 24 hrs; indicative survey spectra showing the changes in elemental composition are shown in Figure SI1 in the Supporting Information. The XPS elemental analysis results on multiple spot sampling on the surface are summarised in Table 2. It is interesting that, despite the significant new phosphorous presence after exposure to BEHP in dodecane solution (in agreement with EDX results; a larger atomic percentage increase is seen in XPS due to its higher surface sensitivity) the iron, carbon and oxygen levels in the two types of sample are similar. The carbon contribution remains large for both samples, attributed to the presence of significant amounts of adventitious carbon species, common with XPS, and possibly of persistent residue from the dodecane solvent. The similar oxygen levels suggest that the phosphorus-containing reaction products are likely to be oxygen rich, 'replacing' or coexisting with the native iron oxide layer on the steel surface.

	XPS atomic percentage / %	
Element	**Polished S355 steel after dodecane exposure**	**S355 after 10 mM BEHP exposure**
C	41.9 ± 1.2	38.7 ± 0.7
O	46.2 ± 1.1	46.4 ± 0.6
P	0.0 ± 0.0	6.4 ± 0.5
Fe	11.9 ± 1.3	8.5 ± 0.6

Table 2: Summary of XPS elemental analysis results for polished and 24-hour BEHP-exposed S355 steel. Errors are evaluated through collection of spectra from multiple sites.

Component peak fitting was conducted on the detailed scans, with the phosphorous 2p peak analysed for its chemical environment. A typical spectrum is shown in Figure 5a. The spectrum is fitted with two peaks that represent one chemical environment, with a spin-orbit splitting of 0.85 eV,[51] and an area ratio of 2:1 between the phosphorous $2p_{3/2}$ and $2p_{1/2}$ peaks. The peaks have a full width half maximum (FWHM) of 1.4 eV, the binding chemical shift of the $2p_{3/2}$ peak is 133.5 ± 0.3 eV, and the standard residual is 0.77. The chemical shift and FWHM are consistent with peaks from iron (III) phosphate or iron (II) phosphate, which share the same shift.[52,53] The formation of inorganic phosphate on the surface is further supported by the phosphorous 2s peak, shown in Figure SI2a in the Supporting Information: significantly the binding energy, 191.0 eV, is too low for adsorbed organic phosphates, typically observed between 192.6 eV (bulk composition) and 191.8 eV (monolayer film).[54]

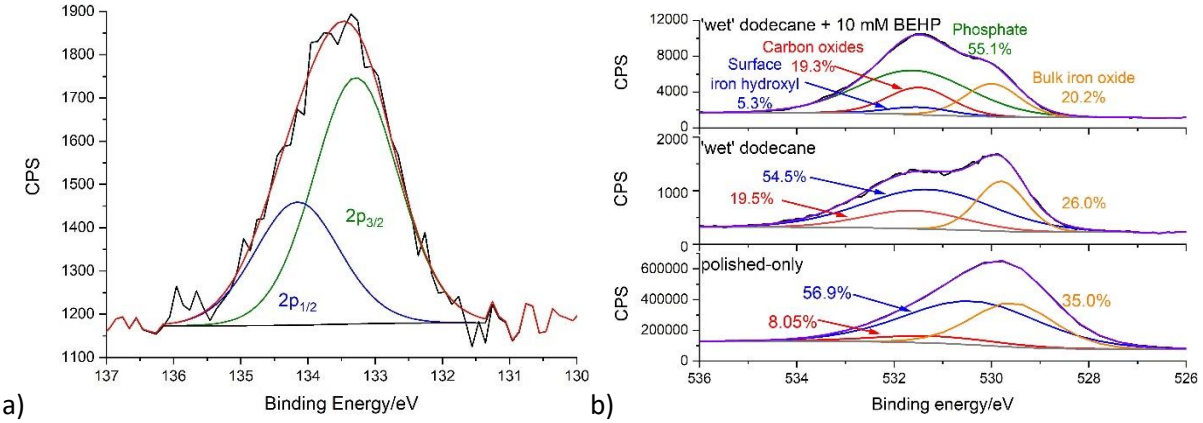

Figure 5: Example photoelectron spectra of **a)** phosphorous 2p peak for a S355 steel surface exposed to 10 mM BEHP in 'wet' dodecane for 24 hrs, and comparison of **b)** oxygen 1s peaks from steel surfaces that have been polished, polished with exposure to 'wet' dodecane for 24 hrs, and polished with exposure to 10 mM BEHP in 'wet' dodecane for 24 hrs. The polished-only sample spectrum was collected under a much higher pass energy (100 eV), leading to a loss of resolution.

The dominant environment in the spectrum from the iron 2p region, shown in Figure SI2b, is iron (III) (with the main Fe $2p_{3/2}$ peak at 711 eV), consistent with the presence of iron (III) phosphate. Although iron (III) also dominates on the untreated surface, significant iron (II) and iron (0) character is evident for both treated and untreated samples.[17] Further deconvolution of the iron 2p spectrum to determine the contribution of an iron phosphate peak (expected at 712.8 eV) was not attempted due to Fe (III) peak domination, making peak separation difficult.

Deconvolution of the oxygen 1s region is shown in Figure 5b. Four peaks are fitted, assigned to bulk iron oxide (in orange), surface iron oxide and hydroxyl groups (blue), carbon oxide species (red), and phosphate species (green), with the latter three overlapping significantly. The three significantly overlapping peaks were separated using the method described by McCafferty *et al.*,[55] in which deconvolution of the carbon 1s peak (Figure SI2c) allows the contribution of oxidised carbon to the oxygen 1s region to be determined. In addition, the atomic percentage and stoichiometric elemental ratios (e.g. for $FePO_4$, the ratio between phosphorous and oxygen is one to four) of the compounds present are used to estimate the contributions of phosphate and bulk iron oxide to the peak.

The approach of McCafferty was also used to interpret the oxygen spectrum obtained from a polished steel surface exposed only to 'wet' dodecane (shown in Figure 5b), using the corresponding carbon 1s peak (Figure SI2c). In comparison to the polished and 'wet' dodecane-exposed samples, the oxygen 1s spectrum from the BEHP-treated surface shows a much smaller contribution from the peak corresponding to bulk iron oxide and surface hydroxyl species. The larger peak weighting to higher binding energy corresponds to the contribution of surface phosphate species; the significant change in the centre of mass of the oxygen peak therefore supports the presence of phosphate species on the iron surface, caused by reaction with BEHP in 'wet' dodecane. This is in contrast to the comparison between a polished-only sample and a 'wet' dodecane-exposed steel surface (Figures 5b, SI2b, and Si2c), where only very minor changes to the chemical environment are seen.

Far-IR RAIRS data from treated surfaces, shown in Figure SI3 in the Supporting Information, indicate strong broad bands around 360 and 600 cm^{-1} and a weaker feature at 475 cm^{-1}. These bands are respectively consistent with Fe-O and phosphate group vibrations,[56–58] supporting the conclusions drawn from the XPS and EDX observations above that phosphate species are present on the treated steel surface.

3.4. Polarised neutron reflectometry (PNR)

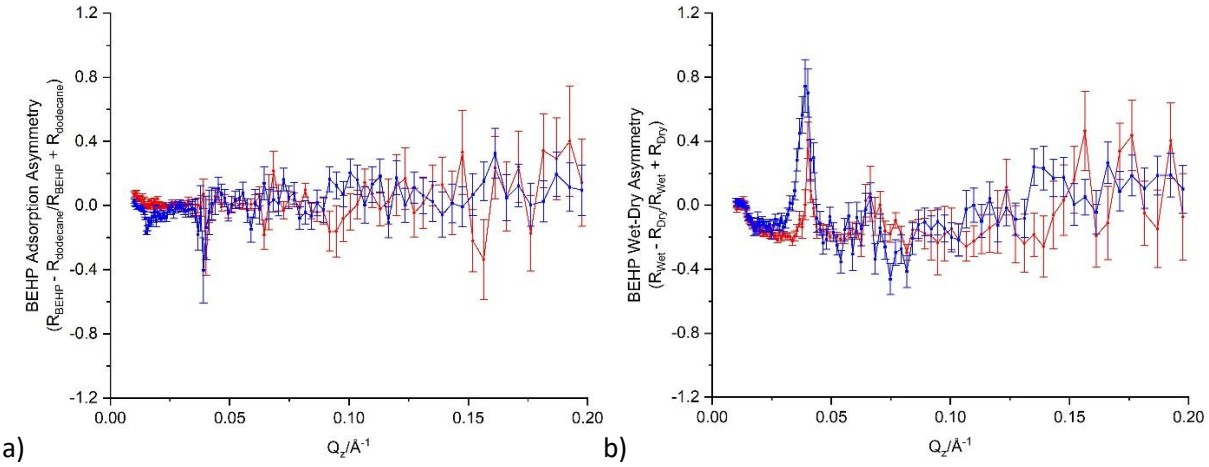

Figure 6: Asymmetry plots of the PNR data for the down (blue) and up (red) spin states, showing **a)** the initial BEHP adsorption (i.e. surface exposed to 2 mM BEHP in dry d-dodecane (24 hrs) vs. surface exposed to dry d-dodecane), and **b)** a comparison of 'wet' and dry BEHP adsorption (i.e. surface exposed to 2 mM BEHP in D_2O-saturated d-dodecane vs. surface exposed to 2 mM BEHP in dry d-dodecane).

PNR was used to monitor the BEHP-steel reaction *in situ*, with a magnetron-deposited iron film used as a model steel surface, in both a dry and 'wet' environment. The iron film surface was first exposed to dry d-dodecane, and then 2 mM BEHP in dry d-dodecane was introduced to the substrate for 24 hrs. The surface was then exposed to 2 mM BEHP in 'wet', D_2O-saturated d-dodecane and measured without a long equilibration time.

To highlight differences in the measured PNR curves under the different conditions asymmetry plots have been used. These plot the difference of two datasets (A_1 - A_0) normalised by the sum of the datasets (A_1 + A_0). If the datasets being compared are the same within error, this yields a flat line at zero, whereas if there are differences in the datasets these are seen as deviations away from zero. The up and down spin states are separately compared for the different chemical conditions.

Figure 6a shows the asymmetry between the surface exposed to 2 mM BEHP in dry d-dodecane vs. pure dry d-dodecane. There is some noise within the data, but there are no significant deviations away from zero indicating that the two datasets are comparable. This shows that no significant adsorbed layer of BEHP or changes in the iron film are measured under these conditions. This is interesting as 2 mM BEHP solution has previously been seen to cause significant reaction with the steel after 24 hrs (evident, for example, by the colouration of the dodecane solution, shown in Figure SI4).

In comparison, Figure 6b shows the asymmetry between the surface exposed to BEHP in 'wet' (D_2O-saturated) d-dodecane vs. dry d-dodecane. In this case, at Q_z values above 0.014 $Å^{-1}$ the asymmetry drops below zero (within error) and a large peak is observed around Q_z = 0.04 $Å^{-1}$. This indicates a significant change when wet d-dodecane is introduced.

To understand these changes we can consider different models for the reflectivity curves. In this case, and based on the observations from the other techniques, we are looking to distinguish between 3 cases: (i) an adsorbed layer of BEHP directly on the iron film, (ii) an adsorbed layer of BEHP on an $FePO_4$ layer, and (iii) just an $FePO_4$ layer, where the organic portion of BEHP is not adsorbed. Figure 7 shows the reflectivity and corresponding SLD profiles for these 3 model cases (lines) with the

measured PNR data shown as data-points. The figure indicates that the closest fit to the data is found for case (iii, red line), where just an iron (III) phosphate ($FePO_4$) layer is included on top of the iron film.

In the comparison in Figure 7, the models produced are based on parameters from models used in similar prior work [25] and have iron/iron oxide layers that are consistent with the pure dry d-dodecane measured in this work. All model parameters used share similar variable ranges. The BEHP monolayer is modelled as 14 Å thick, based on the length of the molecule.[59] Due to slight discrepancies in the data measured, there is some uncertainty around fully fitting these data and the precise model values cannot be extracted from the fits. However, option (iii) clearly offers the best fit, with a single extra layer with an SLD slightly lower than the bulk d-dodecane. This differs from the much lower SLD seen for the BEHP models (i, green line) and (ii, blue line). This larger change in SLD gives rise to more pronounced fringes in the corresponding reflectivity curves, with a very significant elevation in reflection at Q_z approximately 0.13 $Å^{-1}$, which is not in agreement with the measured data, especially in the lower spin state. Note that the structural model needs to fit both spin up and spin down data to be acceptable. It should be noted, that the higher adsorbed layer SLD in option (iii) could also be generated by a mixed layer of BEHP and d-dodecane (i.e. low surface excess). However supporting data from EDX, XPS and far-IR RAIRS lends confidence to an interpretation of $FePO_4$.

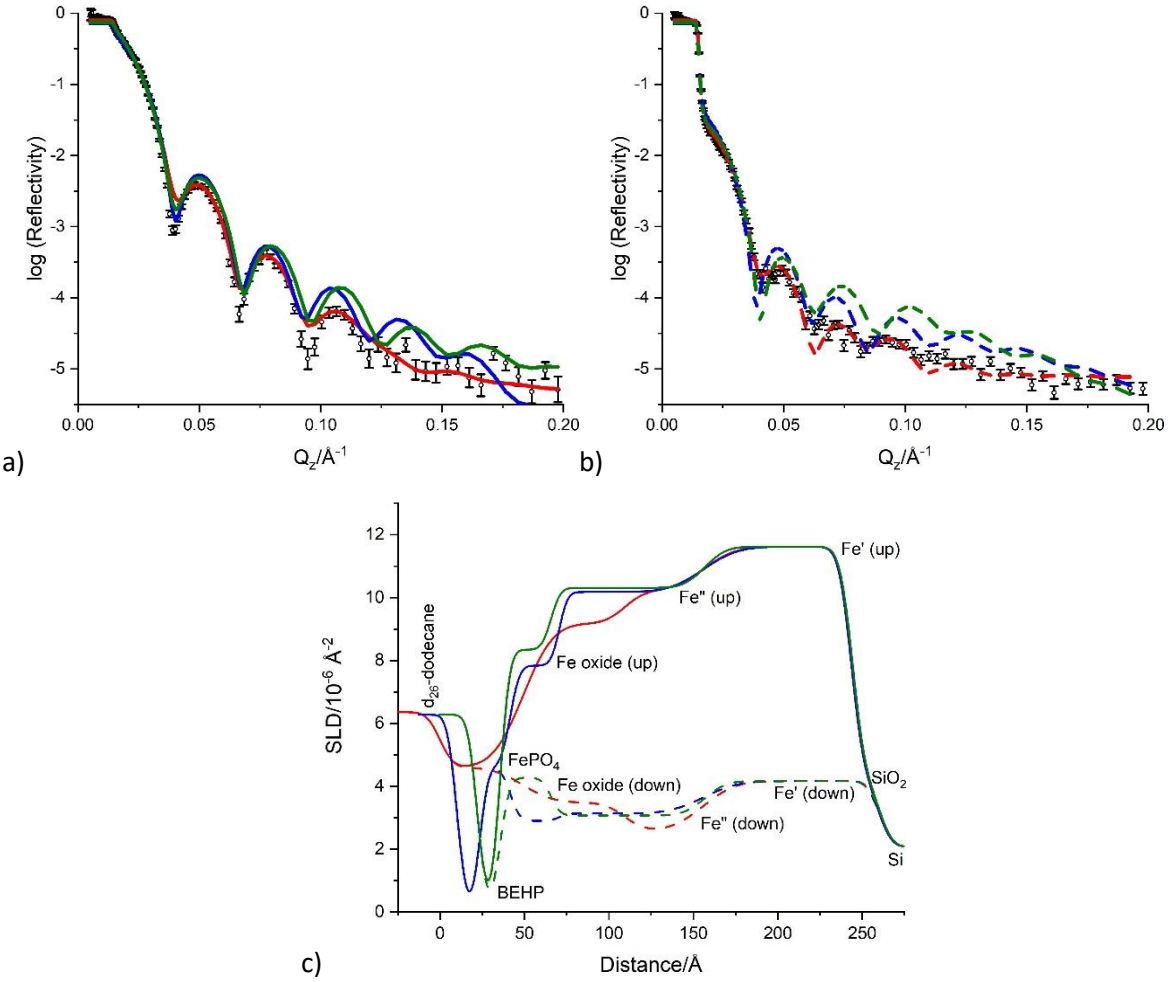

Figure 7: a) Up and b) down spin reflectivity, and c) corresponding SLD curves for three test models to the PNR data for 2 mM BEHP in 'wet' (D_2O-saturated) d-dodecane, having iron and iron oxide layers with: (green) a single BEHP monolayer; (blue) iron phosphate covered by an adsorbed BEHP monolayer; (red) a single iron phosphate ($FePO_4$) layer on top. Solid and dash lines respectively represent up and down spin values for each model.

The lack of reflectivity change on exposure of the iron surface to BEHP in dry dodecane (Figure 6a) is strongly indicative of a lack of affinity between the BEHP and the surface. The subsequent rapid changes when D_2O-saturated dodecane is introduced suggest that the reaction between BEHP and the steel surface, described in the above sections, is initiated by water included in the dodecane solvent. Visible roughening/dulling is again seen for the neutron reflectometry samples, as shown in Figure SI5 in the Supporting Information.

The high sensitivity of PNR to adsorption of protonated species from deuterated solvents, as employed here, strongly suggests that the organic part of the BEHP is not present on the surface. Comparing model fits to the PNR data supports the hypothesis of the phosphate head group detaching from the BEHP molecules and forms a rough solid iron phosphate layer on the surface of the iron film.

The results presented above suggest a possible *in situ* method of phosphating carbon steel surfaces. This method could be useful for coating large steel structures, which cannot be phosphated using traditional methods as they are too big to be completely immersed in phosphating solutions, whereas a surface treatment using BEHP may be more readily facilitated. Inclusion of BEHP in coatings may also allow protective phosphate layers to form when water penetrates the paint, delaying or preventing corrosion of the underlying steel.

3.5. Corrosion resistance study of phosphate-coated carbon steel

Steady-state polarisation curves were used to assess if the surface phosphate formed in the reaction between BEHP and steel affords any corrosion protection, comparable to industrial phosphating of steel surfaces. The polarisation curves were obtained, in artificial seawater, for 'control' S355 steel surfaces (sanded and washed with hexane, then exposed to water-saturated dodecane for 3 hrs), and for surfaces exposed to 2 mM BEHP in water-saturated dodecane for different times. In all cases, the surface appeared to be significantly corroded by the end of the polarisation sweep; an example of the electrode appearance is given in Figure SI6 in the Supporting Information.

Figure SI7 shows several examples of linear polarisation measurements from BEHP-exposed steel samples in artificial seawater, highlighting the significant variation between measurements, even after identical surface preparations. Statistical analysis was therefore used, combining several repeated measurements, in order to assess the effect of the BEHP treatment on the corrosion of the steel surface. Full details of the electrochemical analysis are given in Table SI2 in the Supporting Information. The results are summarised in Table 3: The corrosion potential (E_{corr}), and cathodic (b_c) and anodic (b_a) Tafel slopes are listed, in addition to the corrosion current density (j_{corr}), found from the intersection of the linear cathodic and anodic regions. The protection efficiencies afforded by the BEHP treatment (η) are also listed; these were calculated using:

$$\eta/\% = \frac{j'_{corr} - j_{corr}}{j'_{corr}} \times 100$$

where j'_{corr} is the corrosion current density of the control sample exposed to water-saturated dodecane only. Higher calculated protection efficiencies indicate better corrosion resistance.

BEHP exposure time/hrs	E_{corr}/mV (vs. RHE)	b_c/mV dec^{-1}	b_a/mV dec^{-1}	j_{corr}/μA cm^{-2}	η/%
0 (wet dodecane)	-130 ± 28	408 ± 47	41 ± 7	19 ± 3	0 ± 17
1	-116 ± 18	290 ± 74	28 ± 4	5.0 ± 3.0	74 ± 26
3	-107 ± 39	297 ± 25	25 ± 2	6.1 ± 2.0	69 ± 23
19	-112 ± 18	342 ± 19	31 ± 8	7.8 ± 3.8	60 ± 28
24	-72 ± 21	382 ± 32	28 ± 2	12 ± 0	38 ± 18

Table 3: Electrochemical parameters obtained from polarisation curves of control and BEHP-modified S355 steel electrodes in 3.5% artificial seawater. The indicated errors are standard deviations from repeated measurements, full details of which can be found in Table SI2 in the Supporting Information.

The errors listed in the table are generally large, confirming that there is significant variation between samples, even if they are exposed to BEHP for the same duration. In the case of the corrosion potential, this variation is sufficiently large that there is no significant difference between control and BEHP-treated samples and no clear trend with increasing BEHP exposure time. However, the cathodic and anodic Tafel slopes calculated for BEHP-treated samples are generally lower than those for the control samples. The BEHP-treated samples therefore show reduced corrosion currents and higher protection efficiencies, suggesting that the reaction with BEHP imparts some corrosion resistance to the steel. The protection efficiency is not higher for longer BEHP treatments, which may indicate that the reaction is self-limiting, with the passivating layer that forms preventing further reaction with the surface (which could lead to even greater corrosion resistance).

Standard industrial phosphating of steel is reported to protect the surface from corrosion by forming a cohesive, insoluble passivating layer.[29] Our experiments indicate that the poorly soluble iron phosphate layer formed by the reaction of steel with BEHP,[60] mediated by water, has a similar effect. The layer inhibits anodic iron oxidation and cathodic oxygen reduction by preventing the reactants and products travelling to and from the surface. This method of protection forms an interesting contrast from that described by Yan *et al.*,[38] in which self-assembled monolayers of BEHP dosed from water and ethanol are reported to provide corrosion protection against acidic environments by blocking the hydrogen evolution reaction on the iron surface. Experiments from this work show that the formation of a layer of insoluble iron (III) phosphate on steel can also be similarly effective against corrosion in seawater.

4. Conclusions

Despite showing little affinity to S355 carbon steel in dry aliphatic solvents, bis(2-ethylhexyl) phosphate (BEHP) has been shown to react with the steel surfaces in water-saturated dodecane, forming a layer of iron (III) phosphate that has been characterised using X-ray photoelectron spectroscopy and neutron reflectometry. There is pronounced difference between ‘wet’ and ‘dry’ conditions, even though the practically accessible range of dissolved water concentrations is modest. The formation of the iron (III) phosphate layer may be attributed to water-facilitated hydrolysis of the organophosphate to the inorganic phosphate. We suggest that the modest changes in water content are significant as they reflect changes in the amount of free water (i.e. water not firmly bound to the substrate), and it is this that facilitates hydrolysis.[61] Electrochemical measurements show significant statistical variation. However there are indications that the phosphated steel surface shows a reduced corrosion rate in seawater, indicating that BEHP (applied from wet dodecane) is a candidate for use as a corrosion inhibitor in marine-related applications, giving a similar level of protection to related approaches, but somewhat less than immersion phosphating.[62] The work also highlights the importance of controlling the water content in organic solvents, especially those applied to steel, to encourage or prevent similar reactions taking place between adsorbates and surfaces.

5. Acknowledgments

The authors thank the Royal Dutch Shell Company for the funding and technical support, in particular Dr. Lene Hviid and Dr Damodaran Raghu. JP thanks The Croucher Foundation, Hong Kong, for his fellowship funding. The authors also thank Dr. Petr Motloch at the Department of Chemistry for his help in using the Karl Fischer titrator, Chris Amey at the Cavendish Laboratory for his help in XPS data collection. We thank a referee for the helpful comments to improve the quantitative analysis of the

XPS spectra. We acknowledge the Diamond Light Source and Dr. Gianfelice Cinque for offline-time at the B22 instrument under proposal SM17044, Dr. Adrian Ionescu at the Cavendish Laboratory for his help in magnetron deposition of iron films for neutron experiments, and the beamtime committee at the ISIS Neutron and Muon Source for the beamtime allocation at POLREF (Data DOI: 10.5286/ISIS.E.RB1820335).

6. Data Availability

The raw and processed data required to reproduce these findings are available to download from http://dx.doi.org/10.17632/ykmfygxsr8.1.

7. References

[1] A. Barati-Harooni, A. Najafi-Marghmaleki, A. Tatar, A.H. Mohammadi, Experimental and modeling studies on adsorption of a nonionic surfactant on sandstone minerals in enhanced oil recovery process with surfactant flooding, J. Mol. Liq. 220 (2016) 1022–1032.

[2] A. Barati, A. Najafi, A. Daryasafar, N. Payam, M. Hossein, Adsorption of a new nonionic surfactant on carbonate minerals in enhanced oil recovery: Experimental and modeling study, Chem. Eng. Res. Des. 105 (2016) 55–63. https://doi.org/j.cherd.2015.10.047.

[3] C. Belle, R. Gallo, F. Jacquet, P. Hoornaert, J.P. Roman, The overbasing of detergent additives: The behaviour of promoters and determination of factors controlling the overbasing reaction, Lubr. Sci. 5 (1992) 11–31. https://doi.org/ls.3010050103.

[4] Z. Ahmad, Principles of corrosion engineering and corrosion control, 1st ed., Butterworth-Heinemann, Oxford, 2006. https://doi.org/10.1016/B978-0-7506-5924-6.X5000-4.

[5] R.W. Revie, H.H. Uhlig, Corrosion and Corrosion Control, 4th ed., John Wiley & Sons, Inc., Hoboken, NJ, USA, 2008. https://doi.org/10.1002/9780470277270.

[6] G.H. Koch, M.P.H. Brongers, N.G. Thompson, Y.P. Virmani, J.H. Payer, Costs of corrosion and Preventitive stratigies, Springfield, 2002.

[7] A. Popova, E. Sokolova, S. Raicheva, M. Christov, AC and DC study of the temperature effect on mild steel corrosion in acid media in the presence of benzimidazole derivatives, Corros. Sci. 45 (2003) 33–58. https://doi.org/10.1016/S0010-938X(02)00072-0.

[8] F. Bentiss, M. Lebrini, M. Lagrenée, Thermodynamic characterization of metal dissolution and inhibitor adsorption processes in mild steel/2,5-bis(n-thienyl)-1,3,4-thiadiazoles/hydrochloric acid system, Corros. Sci. 47 (2005) 2915–2931. https://doi.org/10.1016/J.CORSCI.2005.05.034.

[9] I.B. Obot, N.O. Obi-Egbedi, Adsorption properties and inhibition of mild steel corrosion in sulphuric acid solution by ketoconazole: Experimental and theoretical investigation, Corros. Sci. 52 (2010) 198–204. https://doi.org/10.1016/J.CORSCI.2009.09.002.

[10] K.F. Khaled, Molecular simulation, quantum chemical calculations and electrochemical studies for inhibition of mild steel by triazoles, Electrochim. Acta. 53 (2008) 3484–3492.

[11] M.A. Amin, S.S. Abd El-Rehim, E.E.F. El-Sherbini, R.S. Bayoumi, The inhibition of low carbon steel corrosion in hydrochloric acid solutions by succinic acid: Part I. Weight loss, polarization, EIS, PZC, EDX and SEM studies, Electrochim. Acta. 52 (2007) 3588–3600. https://doi.org/10.1016/J.ELECTACTA.2006.10.019.

[12] L. Tang, G. Mu, G. Liu, The effect of neutral red on the corrosion inhibition of cold rolled steel in 1.0 M hydrochloric acid, Corros. Sci. 45 (2003) 2251–2262. https://doi.org/10.1016/S0010-938X(03)00046-5.

[13] J.A. Schreifels, R.E. Morris, N.H. Turner, R.L. Mowery, S.M. Hues, Adsorption of a Metal Deactivator Additive onto Metal Surfaces, Energy & Fuels. 5 (1991) 263–268. http://pubs.acs.org/doi/pdf/10.1021/ef00026a007 (accessed November 26, 2017).

[14] S.M. Tawfik, A.A. Abd-Elaal, I. Aiad, Three gemini cationic surfactants as biodegradable corrosion inhibitors for carbon steel in HCl solution, Res. Chem. Intermed. 42 (2016) 1101–1123. https://doi.org/10.1007/s11164-015-2076-4.

[15] M.H. Wood, R.J.L. Welbourn, T. Charlton, A. Zarbakhsh, M.T. Casford, S.M. Clarke, Hexadecylamine adsorption at the iron oxide-oil interface., Langmuir. 29 (2013) 13735–42.

https://doi.org/10.1021/la4018147.

[16] M.H. Wood, M.T. Casford, R. Steitz, A. Zarbakhsh, R.J.L. Welbourn, S.M. Clarke, Comparative Adsorption of Saturated and Unsaturated Fatty Acids at the Iron Oxide/Oil Interface, Langmuir. 32 (2016) 534–540. https://doi.org/10.1021/acs.langmuir.5b04435.

[17] J. Poon, S.M. Collins, D.C. Madden, H. Sonke, S.M. Clarke, Characterization of Short Time Marine Corroded Surfaces, J. Electrochem. Soc. 166 (2019) C509–C519.

[18] B. He, C.H. Lu, P.J. Han, X.H. Bai, Short-term electrochemical corrosion behavior of pipeline steel in saline sandy environments, Eng. Fail. Anal. 59 (2016) 410–418. https://doi.org/10.1016/j.engfailanal.2015.11.007.

[19] J. Poon, D.C. Madden, M.H. Wood, R. van Tol, H. Sonke, S.M. Clarke, The Surface Chemistry of Almandine Garnet, J. Phys. Chem. C. 124 (2020) 5099–5117.

[20] J.W. Key, S. Zhu, C.M. Rouleau, R.R. Unocic, Y. Xie, J. Kacher, Investigating local oxidation processes in Fe thin films in a water vapor environment by in situ liquid cell TEM, Ultramicroscopy. 209 (2020) 112842.

[21] T. Fujii, Y. Hisada, K. Tohgo, Y. Shimamura, Investigation on nucleation of intergranular stress corrosion cracking in austenitic stainless steel by in situ strain measurement, Mater. Sci. Eng. A. 773 (2020) 138858.

[22] L.I. Fockaert, S. Pletincx, D. Ganzinga-Jurg, B. Boelen, T. Hauffman, H. Terryn, J.M.C. Mol, Chemisorption of polyester coatings on zirconium-based conversion coated multi-metal substrates and their stability in aqueous environment, Appl. Surf. Sci. 508 (2020) 144771.

[23] M. Strebl, M. Bruns, S. Virtanen, Editors' Choice—Respirometric in Situ Methods for Real-Time Monitoring of Corrosion Rates: Part I. Atmospheric Corrosion, J. Electrochem. Soc. 167 (2020) 021510.

[24] M. Luo, Z. Liang, Y. Jia, X.-X. Ye, S. Yan, X. Xia, L. Wang, Z. Li, Z. Jiang, Grain-boundary corrosion of nickel-based alloy by synchrotron radiation technology, Surf. Innov. 7 (2019) 278–283.

[25] M.H. Wood, T.J. Wood, R.J.L. Welbourn, J. Poon, D.C. Madden, S.M. Clarke, An X-ray and Neutron Reflectometry Study of Iron Corrosion in Seawater, Langmuir. 34 (2018) 5990–6002. https://doi.org/10.1021/acs.langmuir.8b00378.

[26] M. Wood, S. Clarke, Neutron Reflectometry for Studying Corrosion and Corrosion Inhibition, Metals (Basel). 7 (2017) 304. https://doi.org/10.3390/met7080304.

[27] A.F. Alshater, A.S. Hakeem, O.W. Saadi, H.M. Ezuber, A. Ebrahim, F. Alhamri, H. Janahi, A correlative study amongst overlay nanostructure and emanating corrosion behavior of pulse-electroplated nanocrystalline zinc on carbon steel, Appl. Nanosci. 9 (2019) 289–304.

[28] J.M. Chovelon, L.E. Aarch, M. Charbonnier, M. Romand, Silanization of Stainless Steel Surfaces: Influence l Application Parameters, J. Adhes. 50 (1995) 43–58.

[29] T.S.N.S. Narayanan, Surface pretreatment by phosphate conversion coatings - A review, Rev. Adv. Mater. Sci. 9 (2005) 130–177.

[30] Y.I. Kuznetsov, N.P. Andreeva, N.P. Sokolova, R.A. Bulgakova, Adsorption of the inhibiting anions on passive iron from an aqueous solution, Prot. Met. 37 (2001) 519–524.

[31] Y.I. Kuznetsov, Progress in the science of corrosion inhibitors, Int. J. Corros. Scale Inhib. 4 (2015) 015–034.

[32] I.B. Obot, D.D. Macdonald, Z.M. Gasem, Density functional theory (DFT) as a powerful tool for designing new organic corrosion inhibitors: Part 1: An overview, Corros. Sci. 99 (2015) 1–30. https://doi.org/10.1016/j.corsci.2015.01.037.

[33] B. El Ibrahimi, A. Jmiai, L. Bazzi, S. El Issami, Amino acids and their derivatives as corrosion inhibitors for metals and alloys, Arab. J. Chem. 13 (2020) 740–771. https://doi.org/10.1016/j.arabjc.2017.07.013.

[34] S.A. Umoren, M.M. Solomon, Synergistic corrosion inhibition effect of metal cations and mixtures of organic compounds: A Review, J. Environ. Chem. Eng. 5 (2017) 246–273. https://doi.org/10.1016/j.jece.2016.12.001.

[35] Z. Yin, M. Kasrai, G.M. Bancroft, K. Fyfe, M.L. Colaianni, K.H. Tan, Application of soft X-ray absorption spectroscopy in chemical characterization of antiwear films generated by ZDDP Part II: the effect of detergents and dispersants, Wear. 202 (1997) 192–201. https://doi.org/10.1016/S0043-1648(96)07273-0.

[36] Z. Yin, M. Kasrai, M. Fuller, G.M. Bancroft, K. Fyfe, K.H. Tan, Application of soft X-ray absorption spectroscopy in chemical characterization of antiwear films generated by ZDDP Part I: the effects of physical parameters, Wear. 202 (1997) 172–191. https://doi.org/10.1016/S0043-1648(96)07272-9.

[37] M.T.L. Casford, P.B. Davies, T.D. Smith, G.L. Bracchi, The Adsorption of Synovene on ZDDP Wear Tracks: A Sum Frequency Generation (SFG) Vibrational Spectroscopy Study, Tribol. Lett. 62 (2016) 1–7. https://doi.org/10.1007/s11249-016-0662-2.

[38] R. Yan, X. Gao, D. Lv, H. Ma, A study on the differences in morphology and corrosion resistance performance between two different bis(2-ethylhexyl) phosphate self-assembled thin films prepared on an iron substrate in water and ethanol solvents, RSC Adv. 6 (2016) 55936–55945.

[39] S.E. Pepper, M. Borkowski, M.K. Richmann, D.T. Reed, Determination of ferrous and ferric iron in aqueous biological solutions, Anal. Chim. Acta. 663 (2010) 172–177. https://doi.org/10.1016/J.ACA.2010.01.056.

[40] K. Fischer, Neues Verfahren zur maßanalytischen Bestimmung des Wassergehaltes von Flüssigkeiten und festen Körpern, Angew. Chemie. 48 (1935) 394–396.

[41] P. Schatzberg, Solubilities of water in several normal alkanes from C7 to C16, 67 (1955) 776–779. https://doi.org/10.1021/j100798a014.

[42] J. Poon, D.C. Madden, M.H. Wood, S.M. Clarke, Characterizing Surfaces of Garnet and Steel, and Adsorption of Organic Additives, Langmuir. 34 (2018) 7726–7737.

[43] S. Tougaard, C. Jansson, Background correction in XPS: Comparison of validity of different methods, Surf. Interface Anal. 19 (1992) 171–174.

[44] R. Matsumoto, Y. Nishizawa, N. Kataoka, H. Tanaka, H. Yoshikawa, S. Tanuma, K. Yoshihara, Reproducibility of XPS analysis for film thickness of SiO2/Si by active Shirley method, J. Electron Spectros. Relat. Phenomena. 207 (2016) 55–59.

[45] T.R. Charlton, R.L.S. Coleman, R.M. Dalgliesh, C.J. Kinane, C. Neylon, S. Langridge, J. Plomp, N.G.J. Webb, J.R.P. Webster, Advances in Neutron Reflectometry at ISIS, Neutron News. 22 (2011) 15–18.

[46] M. Björck, G. Andersson, GenX: An extensible X-ray reflectivity refinement program utilizing differential evolution, J. Appl. Crystallogr. 40 (2007) 1174–1178.

[47] C.F. Majkrzak, K. V. O'Donovan, N.F. Berk, Polarized Neutron Reflectometry, Neutron Scatt. from Magn. Mater. 200 (2006) 397–471. https://doi.org/10.1016/B978-044451050-1/50010-0.

[48] J. Penfold, R.K. Thomas, The application of the specular reflection of neutrons to the study of surfaces and interfaces, J. Phys. Condens. Matter. 2 (1990) 1369–1412. https://doi.org/10.1088/0953-8984/2/6/001.

[49] D.R. Kester, I.W. Duedall, D.N. Connors, R.M. Pytkowicz, Preparation of artificial seawater, Limnol. Oceanogr. 12 (1967) 176–179. https://doi.org/10.4319/lo.1967.12.1.0176.

[50] W. Guo, S. Chen, Y. Feng, C. Yang, Investigations of triphenyl phosphate and Bis-(2-ethylhexyl) phosphate self-assembled films on iron surface using electrochemical methods, fourier transform infrared spectroscopy, and molecular simulations, J. Phys. Chem. C. 111 (2007) 3109–3115.

[51] J.F. Moulder, W.F. Stickle, P.E. Sobol, K.D. Bomben, Handbook of X-ray Photoelectron Spectroscopy, 1st ed., Perkin-Elmer Corporation, Eden Prairie, 1992.

[52] Y. Wang, P.M.A. Sherwood, Iron (III) Phosphate (FePO4) by XPS, Surf. Sci. Spectra. 9 (2002) 99–105.

[53] Y. Wang, D.J. Asunskis, P.M.A. Sherwood, Iron (II) Phosphate (Fe3(PO4)2) by XPS, Surf. Sci. Spectra. 9 (2002) 91–98.

[54] I. Gouzman, M. Dubey, M.D. Carolus, J. Schwartz, S.L. Bernasek, Monolayer vs. multilayer self-assembled alkylphosphonate films: X-ray photoelectron spectroscopy studies, Surf. Sci. 600 (2006) 773–781. https://doi.org/10.1016/j.susc.2005.11.030.

[55] E. McCafferty, J.P. Wightman, Determination of the concentration of surface hydroxyl groups on metal oxide films by a quantitative XPS method, Surf. Interface Anal. 26 (1998) 549–564.

[56] K. Joseph, M. Premila, G. Amarendra, K. V. Govindan Kutty, C.S. Sundar, P.R. Vasudeva Rao, Structure of cesium loaded iron phosphate glasses: An infrared and Raman spectroscopy study, J. Nucl. Mater. 420 (2012) 49–53. https://doi.org/10.1016/j.jnucmat.2011.09.008.

[57] D. Yu, C. Wu, Y. Kong, N. Xue, X. Guo, W. Ding, Structural and catalytic investigation of mesoporous iron phosphate, J. Phys. Chem. C. 111 (2007) 14394–14399.

[58] K. Ding, H. Gu, C. Zheng, L. Liu, L. Liu, X. Yan, Z. Guo, Octagonal prism shaped lithium iron phosphate composite particles as positive electrode materials for rechargeable lithium-ion battery, Electrochim. Acta. 146 (2014) 585–590.

[59] F.H. Allen, O. Kennard, D.G. Watson, L. Brammer, A.G. Orpen, R. Taylor, Tables of bond lengths determined by x-ray and neutron diffraction. Part 1. Bond lengths in organic compounds, J. Chem. Soc. Perkin Trans. 2. (1987) S1–S19. https://doi.org/10.1039/P298700000S1.

[60] S.C. Chang, M.L. Jackson, Solubility Product of Iron Phosphate, Soil Sci. Soc. Am. J. 21 (1957) 265–269. https://doi.org/10.2136/sssaj1957.03615995002100030005x.

[61] T.C. Bruice, A. Tsubouchi, R.O. Dempcy, L.P. Olson, One- and two-metal ion catalysis of the hydrolysis of adenosine 3'-alkyl phosphate esters. Models for one- and two-metal ion catalysis of RNA hydrolysis, J. Am. Chem. Soc. 118 (1996) 9867–9875.

[62] J. Duszczyk, K. Siuzdak, T. Klimczuk, J. Strychalska-Nowak, A. Zaleska-Medynska, Manganese Phosphatizing Coatings: The Effects of Preparation Conditions on Surface Properties, Materials (Basel). 11 (2018) 2585. https://doi.org/10.3390/ma11122585.